

# We are IntechOpen, the world's leading publisher of Open Access books Built by scientists, for scientists

6,900

Open access books available

185,000

International authors and editors

200M

Downloads

Our authors are among the

154

Countries delivered to

TOP 1%

most cited scientists

12.2%

Contributors from top 500 universities



WEB OF SCIENCE™

Selection of our books indexed in the Book Citation Index  
in Web of Science™ Core Collection (BKCI)

Interested in publishing with us?  
Contact [book.department@intechopen.com](mailto:book.department@intechopen.com)

Numbers displayed above are based on latest data collected.  
For more information visit [www.intechopen.com](http://www.intechopen.com)



## Study of Effects of Lightning Strikes to an Aircraft

N.I. Petrov<sup>1</sup>, A. Haddad<sup>2</sup>, G.N. Petrova<sup>1</sup>, H. Griffiths<sup>2</sup> and R.T. Waters<sup>2</sup>

<sup>1</sup>*Istra, Moscow region,*

<sup>2</sup>*Cardiff University,*

<sup>1</sup>*Russia*

<sup>2</sup>*United Kingdom*

### 1. Introduction

It is difficult to avoid thunderstorm regions by aircraft, so that on average every commercial airliner is struck by lightning once per year. Defining test and design criteria of aircraft is becoming important since aircraft safety is increasingly dependent on electronic equipment and the development of new materials (carbon composites, etc.) to replace the metallic airframes.

In-flight statistics show that most strikes occurred 3-5 km above sea level, where the temperature is  $\sim 0^{\circ}\text{C}$  (Uman & Rakov, 2003; Larsson, 2002). There are two different types of lightning strikes to aircraft. The first type is that the aircraft initiates the lightning discharge when it is found in the intense electric field region of a thundercloud, and the second is the interception by the aircraft of an approaching lightning leader. The mechanism for lightning initiation by aircraft is often explained using the “bidirectional leader” theory (Clifford & Casimir, 1982; Mazur, 1989; Mazur et al., 1990; Mazur & Moreau, 1992), which describes the aircraft-initiated lightning process as a positive leader starting from the aircraft in the direction of the ambient electric field; this is followed, a few milliseconds later, by a negative leader developing in the opposite direction. This order of events is a consequence of the lower electric strength of air in the vicinity of a divergent (anode) field. The ambient thundercloud electric field measured under such conditions is typically in the range 50 - 100 kV/m (Marshall & Rust, 1991).

Radome “measles” (coloured spots on the inner radome surface) have been observed in many instances during service (Lalande et al., 1999; Ulmann et al., 1999). Each spot corresponds to a pin hole through the sandwich panel of the radome material. A possible explanation of the origin of these pin holes is that they were caused by breakdown due to double-layer charge accumulation on the radome. However, the physical mechanisms of the occurrence of “measles” are not fully established yet.

The purpose of this chapter was to investigate the physical processes involved in lightning strikes to aircraft and to compare simulation results with other studies involving instrumented aircraft flying in thunderstorms. 3-D electric field calculations were performed to determine the field distributions at the nose of aircraft and inside the dielectric radome (nosecone). The influence of the thickness and dielectric constant of the radome wall on the electric field

penetration inside the radome was also investigated. The screening effect caused by ice and water layers on the radome wall is demonstrated. A new proposal for radome protection is made possible by the development of strips using materials such as non-linear  $ZnO$ , which behave as dielectrics under low-field conditions and acquire properties of conductors if the external electric field exceeds the critical value. Experimental tests of the strips on a real aircraft radome were carried out, and the test results reported in this paper.

## 2. Lightning attachment to aircraft

It was recently reported that about 90% of lightning strikes to aircraft are initiated by the aircraft (Uman & Rakov, 2003). This indicates that the aircraft extremities provide the region of high electric field needed to initiate a lightning discharge by enhancing the ambient electric field. The aircraft geometry and ambient atmospheric conditions are the most important factors in determining the local electric field intensification. Since pressure, absolute humidity and temperature decrease with increasing altitude, the variation of streamer properties with altitude can be inferred from laboratory experiments and incorporated into lightning modelling.

It is inferred from (Petrov & Waters, 1994, 1995) that the electric field needed to initiate a lightning discharge at 4km altitude is only about half of the value at sea level. Calculations show that the required striking distance increases significantly with increasing altitude, causing a corresponding increase in the risk of lightning strikes for aircraft in flight. It is shown, in the following, that ambient electric fields of between 50-80 kV/m can initiate positive leaders at the nose of aircraft at such altitudes.

### 2.1 Aircraft-initiated lightning

Consider the aircraft body as an electrically floating conducting ellipsoid placed in a uniform ambient electric field  $E_0$  (Fig.1). An analytical expression may be obtained for the enhanced electric field in the vicinity of the nose for the case where the major axis is parallel to  $E_0$  (Petrov & Waters, 1994):

$$E(x, a, b) = E_0 \left\{ 1 - \frac{ar \tanh(aA^{1/2}/x) - aA^{1/2}/x}{ar \tanh A^{1/2} - A^{1/2}} + \frac{A}{aA^{1/2}/x} \frac{1}{(x^2/a^2 + b^2/a^2 - 1)(ar \tanh A^{1/2} - A^{1/2})} \right\} \quad (1)$$

where  $A = 1 - b^2/a^2$ ,  $a$  and  $b$  are the half-length and half-width of the ellipsoid and  $(x - a)$  is the distance from the ellipsoid tip.

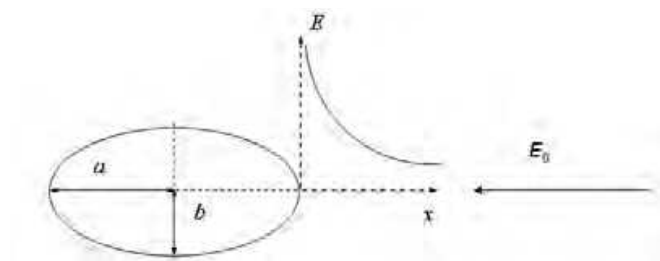


Fig. 1. Aircraft model representation and field intensification.

For given ellipsoid parameters, it is possible to determine the critical value of the ambient electric field which predicts a successful leader development from the aircraft. Using the criteria from (Petrov & Waters, 1994), we find that ambient field magnitudes of  $E_{cr} \approx 50 - 80\text{kV/m}$  (Fig. 2). This is insufficient at sea level to initiate leaders from the aircraft tip. However, at an altitude of 4000m, where the relative air density is around 0.58, triggering of leaders originating from the nose could certainly occur. Ambient fields of 50kV/m agree well with the fields measured inside storm-cloud, consistent with the in-flight measurements of lightning strikes to aircraft (Lalande et al., 1999).

The critical electric field dependence on the half-length of the aircraft, can be approximated with high accuracy using the empirical relationship

$$E_{cr} \cong 570 \cdot a^{-0.68},$$

(2)

where  $a$  is in m, and  $E_{cr}$  in kV/m.

Similar relationship with slightly different coefficient was obtained in (Petrov & D’Alessandro, 2002) for earthed structures.

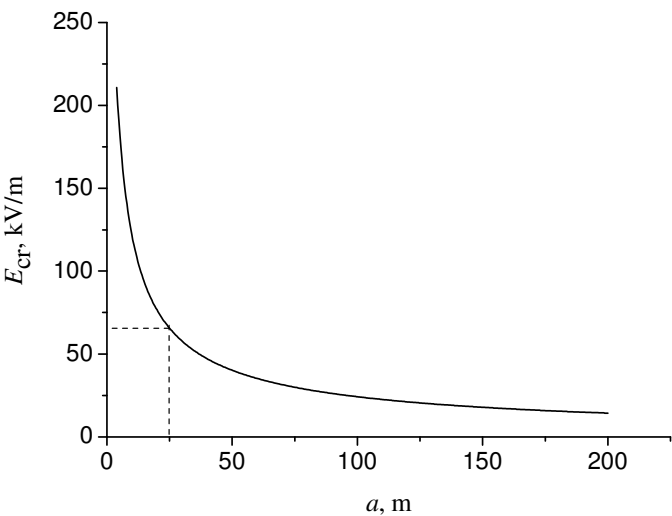


Fig. 2. Critical ambient electric field as a function of aircraft half-length ( $E_{cr} = 65$  kV/m at  $a=25$  m,  $b=3\text{m}$ ).

2.2 Aircraft-intercepted lightning

An aircraft can, in principle, intercept an approaching lightning leader, although no direct evidence is available. Nevertheless, in this case, the striking distance concept usually used for earthed structures may be applied to estimate the risk factor. The striking distance and the probability of lightning strikes are functions of aircraft geometry and lightning current. Electric field intensification of the field of a nearby lightning leader as a function of the distance from the aircraft tip is presented for different values of lightning peak current in Fig. 3. The aircraft is again modelled as an ellipsoid with half-width of 3m and half-length of 25m. The lightning leader channel is modeled by a charge per length,  $q$ , and leader tip charge,  $Q$ , at a distance,  $S$ , from the aircraft. The values for  $q$  and  $Q$  correspond to a prospective lightning return stroke current  $i_0$ , evaluated from (Petrov & Waters, 1995), i.e.

$$q \approx 0.43 \cdot 10^{-6} i_0^{2/3} \quad [\text{C/m, A}], \tag{3}$$

Note that there are similar relationships between the leader channel charge and the return stroke current obtained from other models. A review of data concerning this relationship was made in (Cooray et al., 2004).

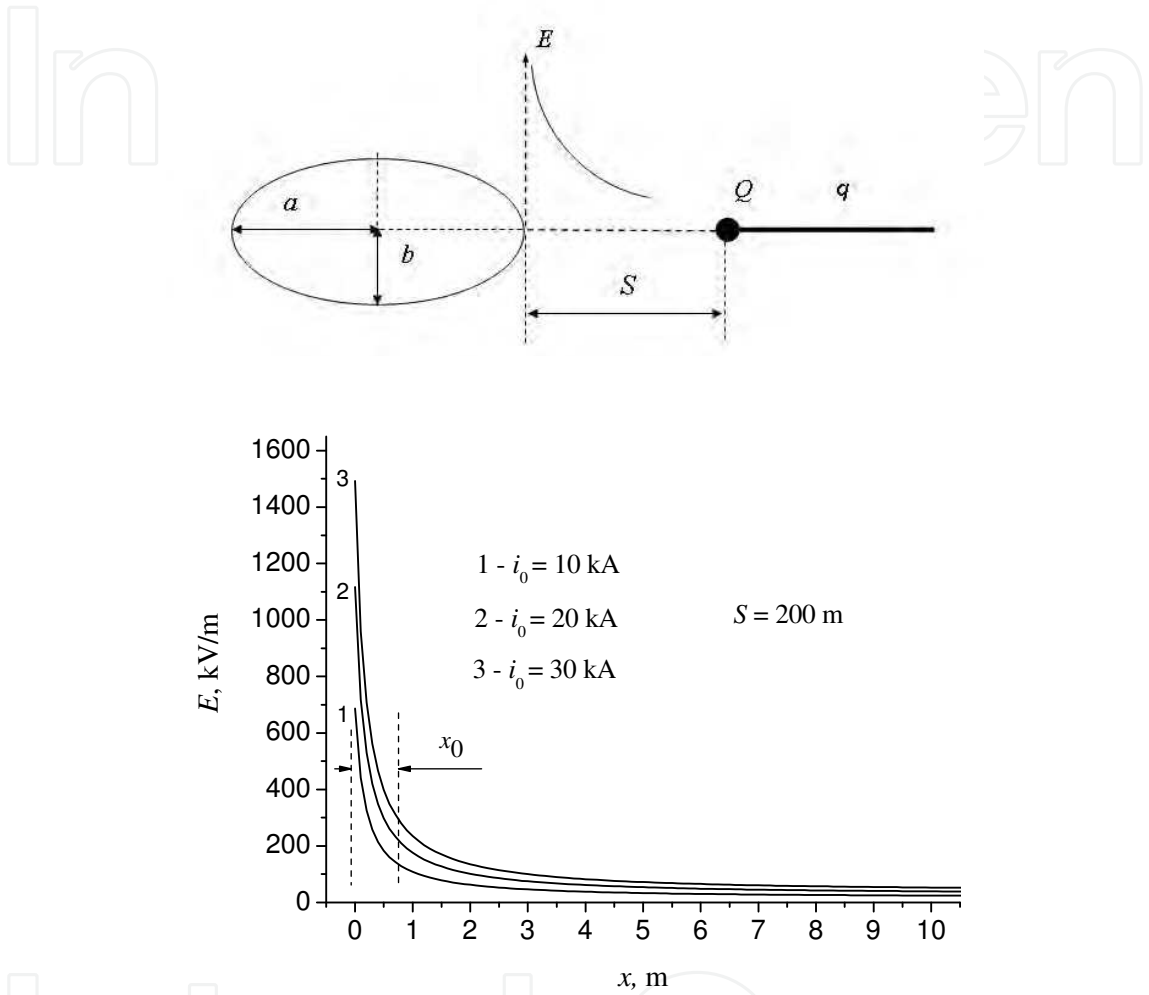


Fig. 3. Electric field intensification as a function of distance from the aircraft tip for different values of lightning peak current.

In Fig. 4, the striking distance of negative lightning to the aircraft as a function of lightning current is presented for different altitudes above sea level. Note, that for positive lightning, these distances are substantially less than those obtained for negative polarity lightning (Petrov & Waters, 1999).

A semi-quantitative estimate of the risk of lightning strike interception by an aircraft can be obtained from the concept of attractive area as used in lightning protection standards for ground structures, which can also be derived from lightning models (Petrov & Waters, 1995). For a grounded structure of the size of a commercial aircraft, the attractive area to a powerful lightning stroke of 100kA is of the order of 0.2km<sup>2</sup>. At 4000m altitude, this would increase to 0.6km<sup>2</sup>. Then, if the flash activity (cloud-cloud and cloud-ground) is  $N$

flashes/ $\text{km}^2/\text{s}$ , the aircraft would be expected to intercept  $0.6N$  flashes/s. Active storms can generate 2 flashes/minute over  $10 \text{ km}^2$ , which suggests an interception rate of 1 per 500s at the heart of a storm.

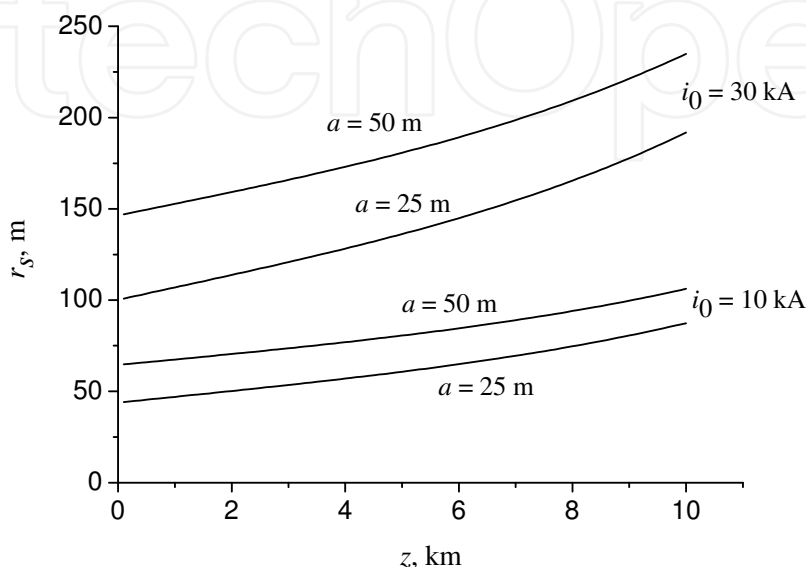


Fig. 4. Lightning interception distances by aircraft of different half-lengths as function of altitude above sea level for lightning peak current values of 10 kA and 30 kA.

### 3. Electric field around radomes

Radar and communications antennae are usually located at the nose or tail of the aircraft where lightning is most likely to attach. Lightning strikes damage non-metallic radomes, so the diverter strips were developed to mitigate this problem. The diverter strips screen the lightning induced electric fields on the antenna surface, i.e. they move the internal streamer initiation points forward so that strips cause the collapse of electric field inside the radome. Solid strips (permanent conductors) have been used for this purpose. However, they were found to interfere with antenna radiation patterns because they usually extend beyond the antenna. For this reason, segmented diverter strips were developed to reduce the interference effects on antenna radiation (Amason et al., 1975; Plumer & Hoots, 1978). Although they have better electromagnetic transparency for radar, segmented strips need a significant voltage gradient to light up, and their efficiency needs to be further proved.

#### 3.1 Electric field distribution at radome without strips

For a simplified analytical calculation of 3-D electric field, consider a hemi-spherical radome with thickness  $d$  placed in uniform field  $E_0$  (Fig. 5). This is equivalent to the floating dielectric hollow sphere (permittivity  $\epsilon$ , internal and external radii  $a$  and  $b$ ) placed in the electric field  $E_0$ .

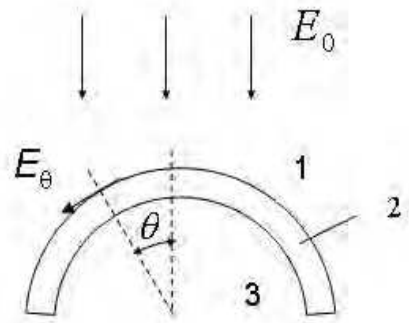


Fig. 5. Simplified model of radome exposed to electric field  $E_0$ .

The analytical solution of Laplace's equation for the potentials outside the sphere (Region 1) and inside the sphere (Region 3) can be obtained as:

$$\begin{aligned}\varphi_1 &= -E_0 \cos \theta \left( r - \frac{A}{r^2} \right), & [r > b]; \\ \varphi_3 &= -BE_0 r \cos \theta, & [r < a]\end{aligned}\quad (4)$$

and the potential inside the dielectric layer (Region 2)

$$\varphi_2 = -CE_0 \cos \theta \left( r - \frac{D}{r^2} \right), \quad [a < r < b] \quad (5)$$

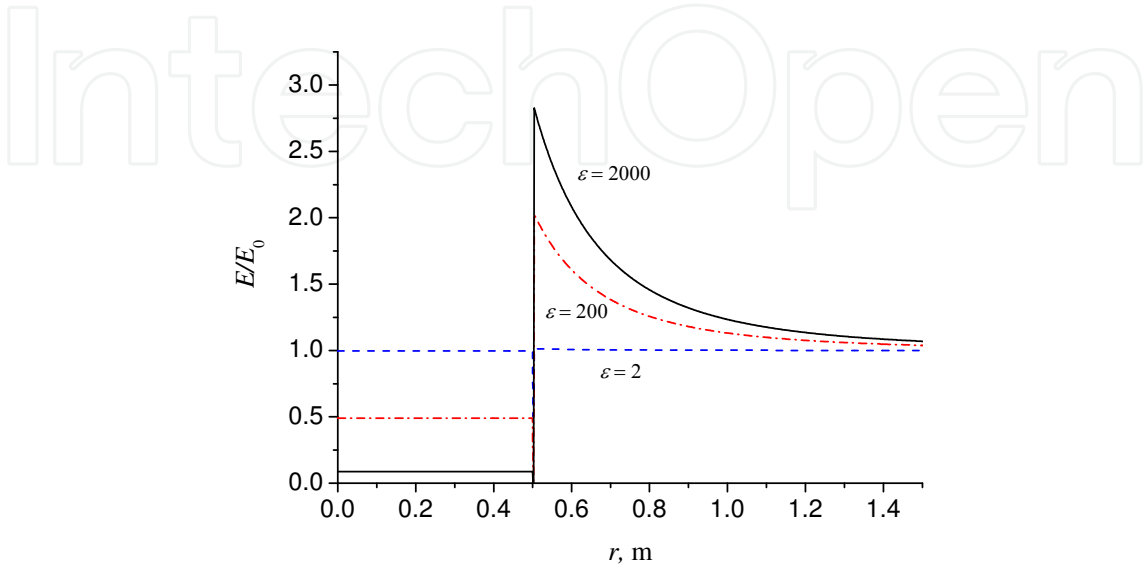
where  $A, B, C, D$  are constants determined from the continuity condition for  $\varphi$  and  $\varepsilon \partial \varphi / \partial r$  on the boundaries of regions 1-2 and 2-3. Calculation of these constants leads to the following expressions:

$$\begin{aligned}A &= a^3 \left\{ 1 - \frac{3[1 + 2\varepsilon + (\varepsilon - 1)b^3 / a^3]}{(\varepsilon + 2)(2\varepsilon + 1) - 2(\varepsilon - 1)^2 b^3 / a^3} \right\}, \\ B &= \frac{9\varepsilon}{(\varepsilon + 2)(2\varepsilon + 1) - 2(\varepsilon - 1)^2 b^3 / a^3}, \\ C &= \frac{3(2\varepsilon + 1)}{(\varepsilon + 2)(2\varepsilon + 1) - 2(\varepsilon - 1)^2 b^3 / a^3}, \quad D = -\frac{b^3(\varepsilon - 1)}{2\varepsilon + 1}.\end{aligned}\quad (6)$$

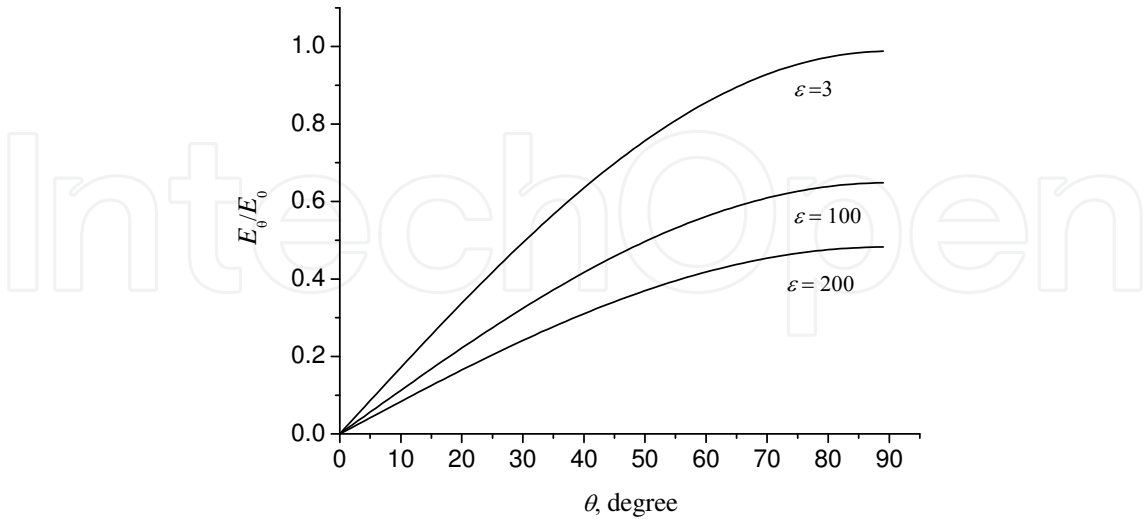
For the radial and tangential components of the electric field outside the radome surface, we obtain

$$\begin{aligned}E_r &= -\frac{\partial \varphi}{\partial r} = E_0 \cos \theta \left( 1 + \frac{2A}{r^3} \right), & [r > b] \\ E_\theta &= -\frac{1}{r} \frac{\partial \varphi}{\partial \theta} = -E_0 \sin \theta \left( 1 - \frac{A}{r^2} \right), & [r > b]\end{aligned}\quad (7)$$

In Figs. 6a and 6b, the radial and tangential electric field distributions are presented for radomes having different dielectric constants. It is seen that the screening of the electric field by the radome itself increases when the dielectric constant of the radome material increases.



a. Radial electric field distribution inside and outside the one-layer semi-spherical radome



b. Tangential electric field distribution inside the one-layer semi-spherical radome

Fig. 6. Electric field distribution in the vicinity of a radome.



## i. 2-layer radome wall

By analogy, the potentials and electric fields may be obtained for the 2-layer radome wall placed in the field  $E_0$ :

$$\begin{aligned}
 \varphi_1 &= -E_0 \cos \theta \left( r - \frac{A}{r^2} \right), & [r > c] \\
 \varphi_2 &= -CE_0 \cos \theta \left( r - \frac{D}{r^2} \right), & [a < r < c] \\
 \varphi_3 &= -FE_0 \cos \theta \left( r - \frac{G}{r^2} \right), & [b < r < a]; \\
 \varphi_4 &= -BE_0 r \cos \theta, & [r < b]
 \end{aligned} \tag{8}$$

$$A = c^3 - C(c^3 - D), \quad B = \frac{F(b^3 - G)}{b^3}$$

$$C = \frac{3\varepsilon_1 c^3}{2\varepsilon_1(c^3 - D) + \varepsilon_2(c^3 + 2D)},$$

$$D = \frac{a^3 \left[ 1 - (\varepsilon_2 / \varepsilon_3)(a^3 - G) / (a^3 + 2G) \right]}{1 + 2(\varepsilon_2 / \varepsilon_3)(a^3 - G) / (a^3 + 2G)},$$

$$F = \frac{C(a^3 - D)}{a^3 - G}, \quad G = \frac{b^3(1 - \varepsilon_3 / \varepsilon_4)}{1 + 2\varepsilon_3 / \varepsilon_4},$$

where  $b < a < c$ , with  $b$  the internal radius of the inner layer,  $a$  and  $c$  are the internal and external radii of the exterior layer,  $\varepsilon_1, \varepsilon_2, \varepsilon_3, \varepsilon_4$  are the dielectric constants of outside medium (air), exterior and interior layers, and inside medium (air), accordingly.

Radial and tangential components of the electric field outside the radome surface are expressed by

$$\begin{aligned}
 E_r &= -\frac{\partial \varphi}{\partial r} = E_0 \cos \theta \left( 1 + \frac{2A}{r^3} \right), & [r > c] \\
 E_\theta &= -\frac{1}{r} \frac{\partial \varphi}{\partial \theta} = -E_0 \sin \theta \left( 1 - \frac{A}{r^2} \right), & [r > c]
 \end{aligned} \tag{9}$$

In Fig. 7, the electric field distributions inside and outside the two-layer semi-sphere radome are presented for different values of dielectric constants of layers. It can be seen that the field intensification at the tip of a radome increases with the dielectric constant of the radome layers.

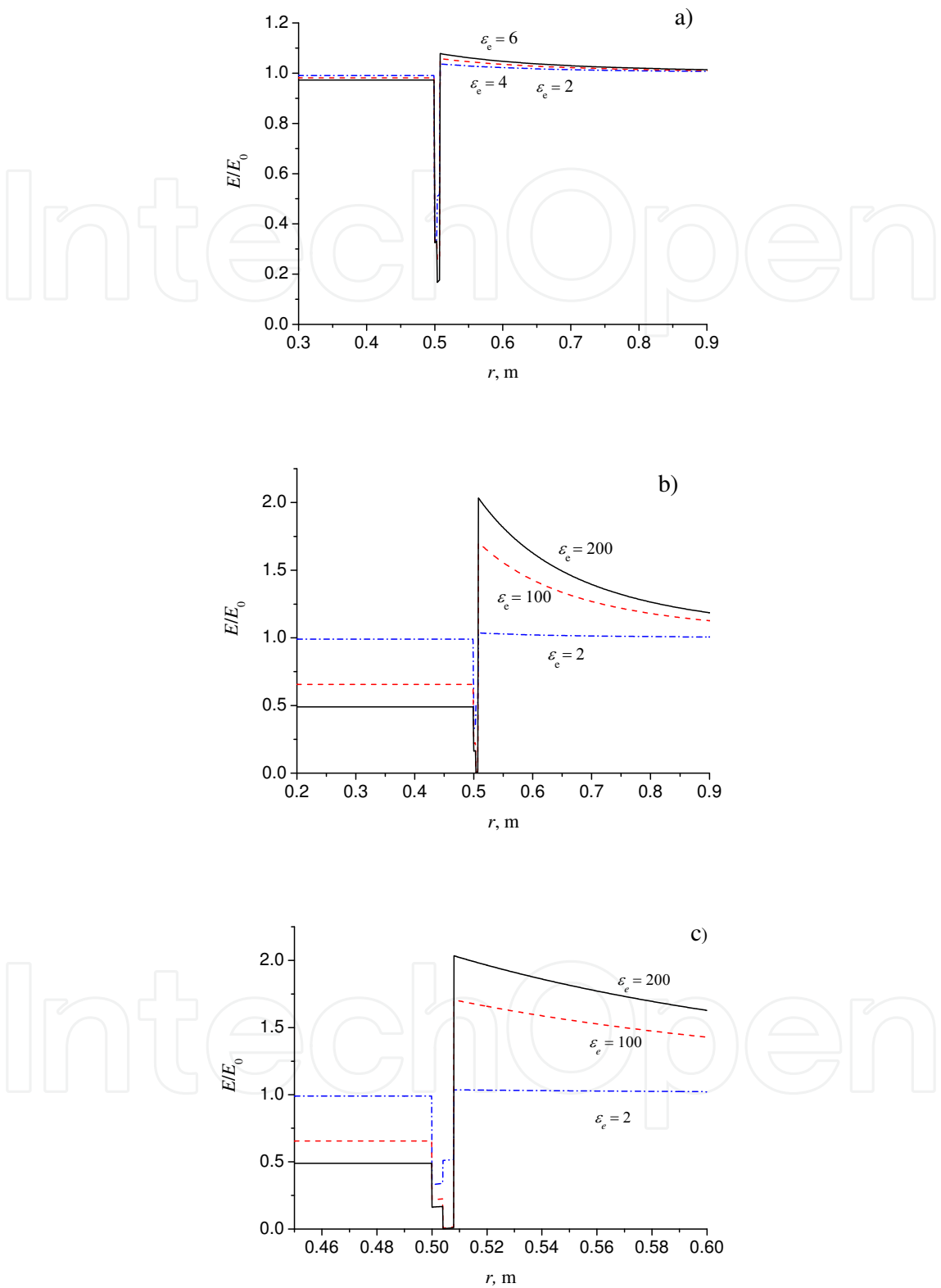


Fig. 7. Electric field distribution inside and outside the two-layer semi-sphere radome: a)  $\epsilon_i=3$  for internal layer;  $\epsilon_{e1} = 2, \epsilon_{e2} = 4, \epsilon_{e3} = 6$  for external layer; b)  $\epsilon_i = 3; \epsilon_{e1} = 2, \epsilon_{e2} = 100, \epsilon_{e3}=200$ ; c) expanded scale of b).

## ii. Effect of ice and water layers

In in-flight environmental conditions, the radome may be covered by ice or water layers. The tests on radomes in rain and icing conditions were conducted recently (Hardwick et al., 1999, 2003), and it was shown that the ice layers increase the light up voltages by a factor 2 to 3.

Calculations of the electric field distributions in the case of ice and water on the radome surface show that radome produces significant shielding effect (Fig. 8). In this case, the lightning leader can be initiated from the radome tip, so the strips will not operate as usual. In Fig. 8, the electric field distributions are presented for different values of permittivity of the radome wall material. The radar is represented by a conducting hemisphere having a radius of 0.2m. Note, that for a wide range of frequencies, the dielectric constants of water and ice are equal to  $\epsilon_{H_2O} = 87.9$  and  $\epsilon_{ice} = 99$ , respectively (Handbook of Chemistry, 2001).

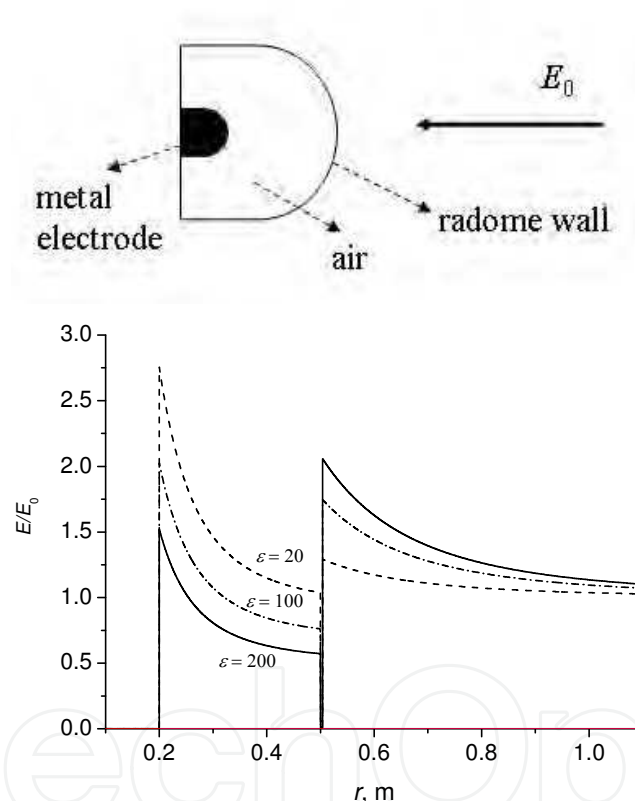


Fig. 8. Electric field distribution inside and outside the hemisphere radome with different dielectric constants of radome material.

## 3.2 Electric field shielding effect of strips

As was shown above, the electric field inside a dielectric radome is not disturbed significantly by the radome wall itself, so the radome does not produce screening effects. Low-level shielding permits the inception of a discharge from the internal electrode, so the solid strips are usually used to produce the shielding effect. However, high quality shielding has undesirable interference effects on antenna radiation. Therefore, the optimal length and number of strips should be determined. In the following, we consider a conical shaped

radome with a base diameter of 0.7m (Fig. 9). For this radome, electric field measurement results at its base were reported (Ulmann et al., 2001; Delannoy et al., 2001), which allows comparison of simulations with experimental data. Here, solid strips were considered as inclined isolated rods in a uniform external electric field, since the analytical expressions for the electric field distribution exist in this case. In Fig. 10, the electric field at the radome base is shown as a function of strip length for different numbers of strips. It can be observed that the electric field at the radome base decreases by 50 % if 6 solid diverter strips of 0.4m length were installed on the radome surface. This is in good agreement with the measurements (Ulmann et al., 2001).

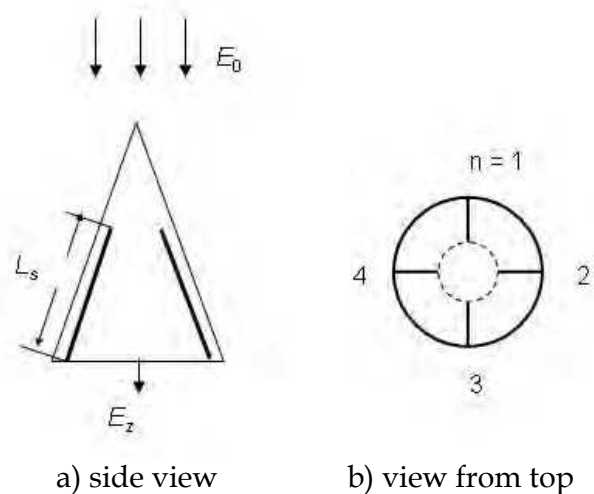


Fig. 9. A conical radome with conducting solid strips:

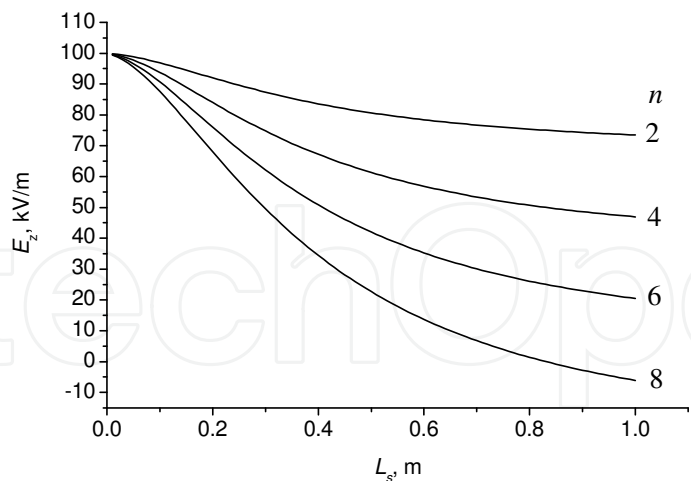


Fig. 10. Calculated electric field at the radome base as a function of strip length for different numbers of strips

4. Laboratory lightning impulse tests

Preliminary tests on a radome, used on a commercial aircraft, with a thickness of ~5 mm, a diameter of ~ 1.6 m and having six solid strips of 1m length were performed in the high

voltage laboratory at Cardiff University. Lightning impulses of 1.2/50 shape, positive and negative polarity, were applied to the output electrode (sphere of 10cm diameter or rod with spherical end of 1.2cm diameter), which was placed at different distances (10-30 cm) from the surface of the radome. Breakdown channels were recorded using a video-camera having a picture rate of 50 fps.

#### 4.1 Segmented diverter strips

Tests were also conducted on two commercially available segmented diverter strips of one meter length each. The diverter strips were attached to the aircraft radome surface for testing. It was found that the diverter with smaller buttons (segment diameter 1.524 mm) has higher breakdown voltage.

The segmented diverters had breakdown voltages of 50-60kV while the time to breakdown  $t_{br}$  varied between 3 and 7 $\mu$ s. This corresponds to leader velocities  $v_l$  in the range 15 to 30 cm/ $\mu$ s, which is ten times higher than usually registered leader velocities in long air gaps. Dependence of the applied voltage on the polarity is weak, if the rod-type high voltage electrode is placed close (~10-15cm) to the strip end.

Although the segmented strips have good diversion properties, tests have shown problems with multi-impulse lightning strikes. After a number of strikes, damage was observed on the strip buttons (Fig. 11). However, the resistance of the strips after tests was still more than 600 M $\Omega$ . This indicates that the discharge current mainly flows not through the strip buttons but in air over the strip.

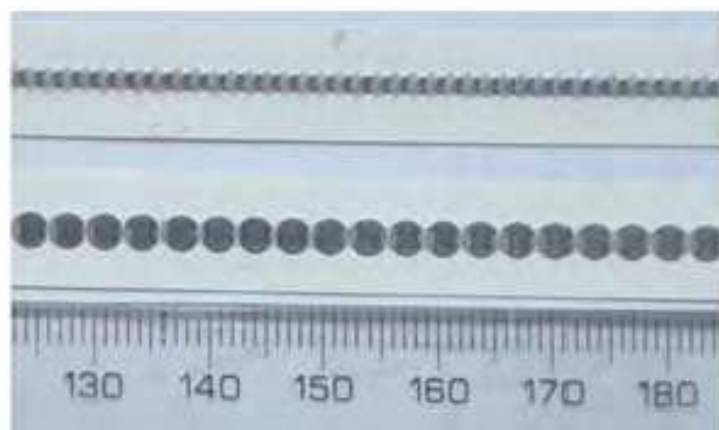


Fig. 11. Segmented diverter strips after the test.

#### 4.2 Isolated multiple-electrode diverter

Isolated rings or disks with diameters of 17mm and 20mm with a separation of 5-15cm were mounted on the radome surface with the help of dielectric tape. These types of strips have several advantages: (a) they have negligible interference effects on antenna radiation due to the small total surface of metal elements and (b) they do not initiate a leader discharge before an approaching lightning leader streamer zone attaches to the radome surface. Both positive and negative polarity impulses of amplitude 200-250 kV were applied to gaps of 10-20cm between the electrode and the radome tip (Fig. 12 and Fig. 13).

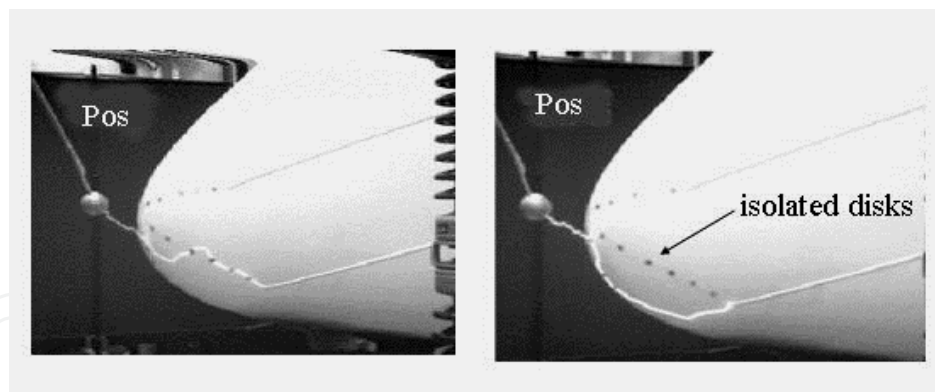


Fig. 12. Influence of isolated disks on the trajectory of breakdown under positive impulse

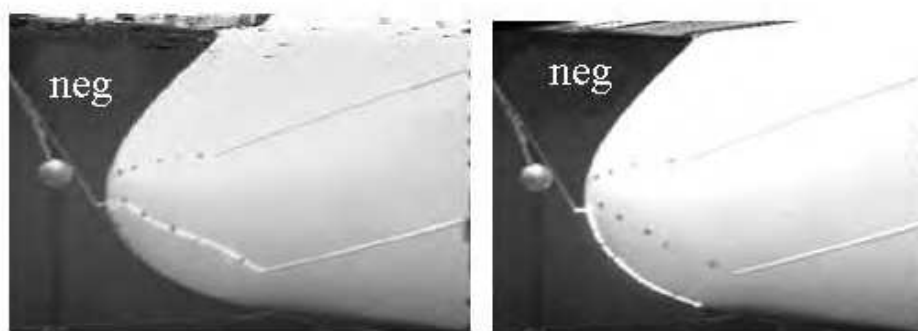


Fig. 13. Influence of isolated disks on the trajectory of breakdown under negative impulse

Breakdown occurs between the electrode and the closest point on the radome surface, propagating further along the radome surface until the end of the solid strip, even if the air gap distance between the electrode and the end of the solid strip is shorter. This indicates that the breakdown voltage along the surface of the radome is lower than the breakdown voltage in an air gap. The time to the surface breakdown was  $t_{br} \sim 30\text{--}50 \mu\text{s}$  depending on the distance between the electrode and the end of the solid strip on the radome wall. This corresponds to a leader velocity  $v_l \sim 2 \text{ cm}/\mu\text{s}$ , which is usually recorded in long air gaps. In the case of the isolated multiple-electrode diverters, the time to breakdown decreases by a factor of 3–4, i.e. the leader velocity becomes  $v_l \sim 6\text{--}8 \text{ cm}/\mu\text{s}$ . The decrease of the breakdown time indicates that simultaneous development of the discharge in the gaps between different isolated electrodes.

The light up electric field was about  $3.3 \text{ kV}/\text{cm}$ , which is close to typical light up voltages with  $D$  waveform for the segmented strips (Hardwick et al., 1999).

Tests have shown that the isolated electrode strips divert the discharge channel of both polarities. Leaders develop along the surface without any damage to it. For the same applied voltage, the breakdown gap with the isolated multiple-electrode diverter strip can be twice as long as the gap without strip. The diversion ability of isolated multiple-electrode diverter strip is higher for negative polarity discharge than for positive discharge (Figs. 12, 13). This is due to different mechanisms of breakdown for negative and positive polarity discharges (Petrov & Waters, 1999).

### 4.3 Flashover across the radome wall

The discharge develops along the surface of the radome even if the air gap distance between the output electrode and the termination of the strips is shorter. This indicates that the breakdown voltage along the dielectric surface is lower than the breakdown voltage in air.

A leader discharge can be initiated from the internal radar antenna. In the model, the antenna was represented by a grounded metal hemisphere at the radome base. The leader channel from the antenna was modeled as a metal rod of different lengths connected with the antenna.

The laboratory experiments have shown that both positive and negative polarity discharges can cause a puncture through the radome wall when the internal electrode (antenna) extends beyond the strips and, hence, when it is no longer screened.

In Fig. 14, the flashover path can be seen initially propagating along the surface and then passing through the radome wall to the internal grounded electrode. The distance from the surface puncture point to the grounded outer electrode was only 7.5 cm. This indicates that a voltage drop of less than 20 kV is sufficient to cause a flashover across the radome wall.

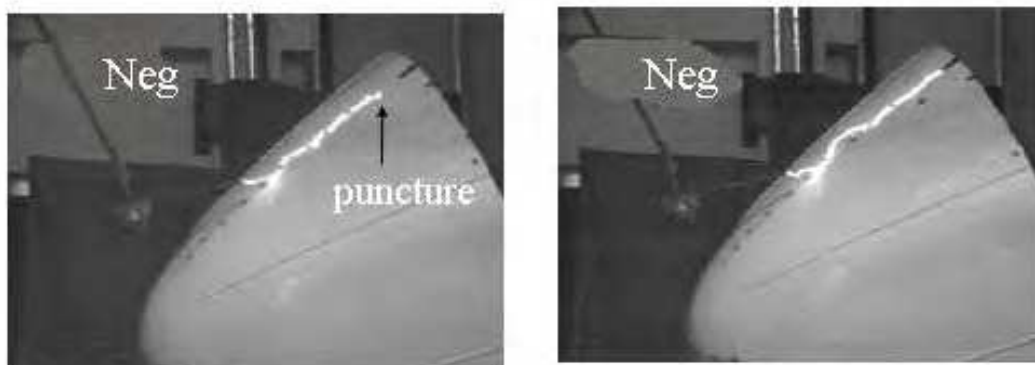


Fig. 14. Puncture through the radome wall with an earth electrode inside the radome.

### 4.4 Diverter strips with ZnO material

Segmented strips consisting of ZnO material between Al segments of 3x3 mm size were designed and tested (Fig. 15). Experiments have shown that the influence of ZnO material on the discharge properties of strips depends on the distances between the segments. Although no significant influence was observed for gaps  $d > 10$  mm, at  $d \sim 1-3$  mm, the influence of ZnO material becomes significant. The competitive breakdown tests showed that all discharges pass through the strip consisting of ZnO material, which indicates that electric fields created between the segments are sufficient for the ZnO material to become conductive. The breakdown time for these strips is comparable to that of commercial segmented strips. The velocity of leader propagation increases 4-5 times in comparison to the velocity of the surface leader discharge without the strips.



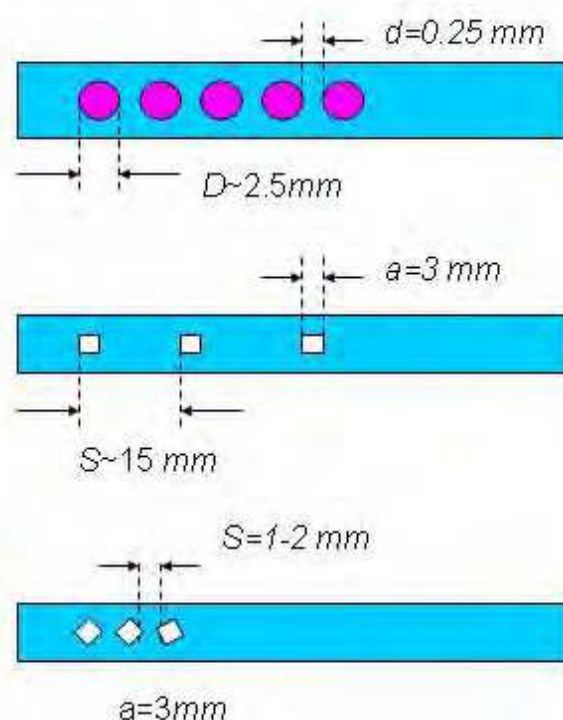


Fig. 15. Designed diverter strips with ZnO material.

### 5. 3D numerical computation of electric field around radomes

The electric field and potential distributions inside and outside the aircraft radome placed in an external electric field were analyzed using COULOMB software which is based on the boundary element method. This results of this analysis were used to determine the necessary number and length of strips to be utilized to provide the radome with the optimised lightning protection using strips.

A simulation model of the aircraft radome having a hemispherical shape placed in a uniform ambient electric field was used in a plane-plane gap (Fig. 16). The gap length is 5.2 m and the applied voltage is 2 MV. The dielectric hemispherical radome is placed on top of a metal cylinder of 1.5 m length to simulate the end of the fuselage. The hemispherical radome has a radius of 0.5m and a thickness of 4mm and a dielectric constant  $\epsilon_r = 10$ . Solid strips of 1cm width and 3mm thickness were considered. The segmented strips have a 5mm diameter and a 3mm thickness of and a gap distance of 1mm. The distance between the radome tip and the upper electrode is 2m. The distance between the bottom of the cylinder and the bottom electrode is 1.2m.

Fig. 17 shows the solid and segmented strips attached to the radome surface. Fig. 18 shows examples of computed voltage contours.



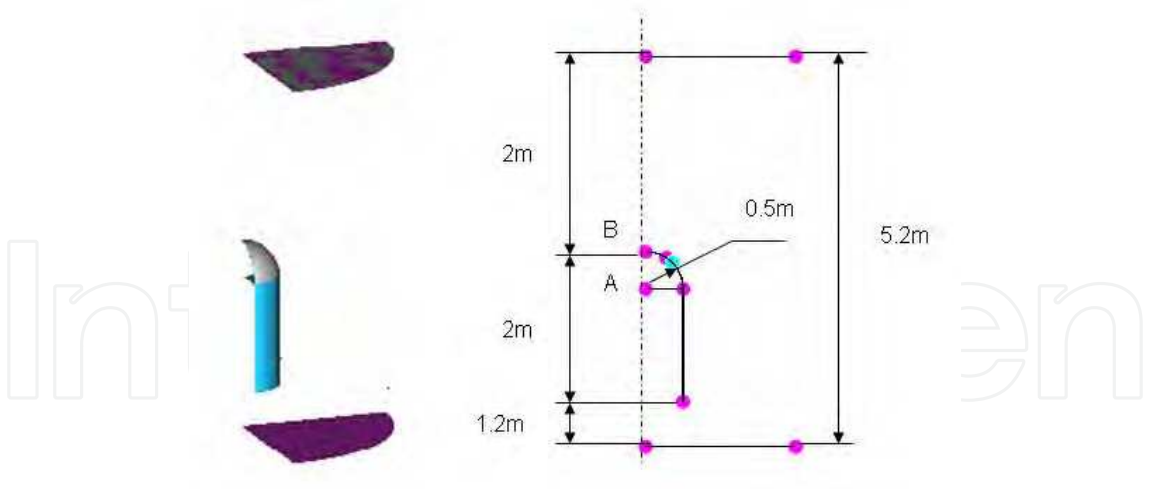


Fig. 16. Model representation: semi-spherical radome.

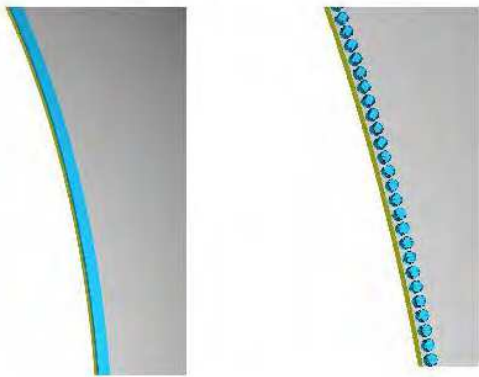


Fig. 17. Modeled solid (thickness: 3mm, width: 10 mm) and segmented (thickness: 3mm, radius: 2.5 mm, gap: 1 mm) strips.

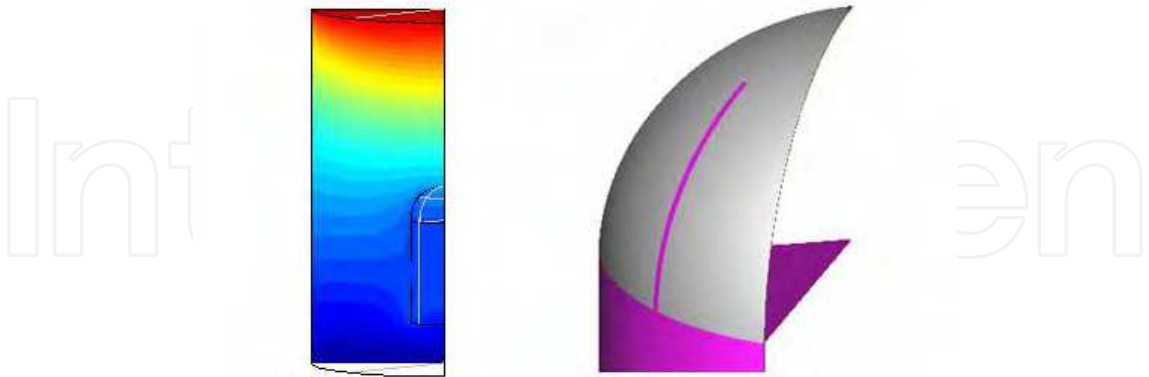


Fig. 18. Voltage contour and section of a radome with a solid strip.

Tables 1 and 2 summarise the computed magnitudes of electric field at the radome base and tip. It can be observed that the shielding effect increases with the length of solid strips and the number of strips. The electric field at the base of the radome is only 50% of the external field if 6 solid strips of 0.5m length are used. Segmented strips do not produce any visible shielding effects.

Detailed analysis has shown that an increase of the number of solid strips results in a decrease in the electric field at the base of the radome. On the other hand, the electric field was forced out to the frontal area of the radome, so that too strong shielding of the internal electrode can cause undesired field intensification at a radome front. This is a disadvantage with solid strips, in addition to their interference effect on the radiation field from the antenna. In the case of segmented strips, there is no shielding effect. This indicates that there will be no interference effect with the radiation field until the breakdown along the strip takes place, under which condition the strip behaves like a conductor.

	Solid strips					
Number of strips	4		6		8	
Length, m	0.25	0.5	0.25	0.5	0.25	0.5
$E(A),$ $kV/m$	482	335	456	270	435	226
$E(B),$ $kV/m$	493	534	515	588	524	570

Table 1. Electric field magnitudes at radome base (point A in Fig.16) and radome tip (point B in Fig. 16) for different numbers of solid strips.

	Segmented strips					
Number of strips	4		6		8	
Length, m	0.25	0.5	0.25	0.5	0.25	0.5
$E(A),$ $kV/m$	517	524	526	508	551	515
$E(B),$ $kV/m$	477	472	481	497	477	475

Table 2. Electric field magnitudes at radome base (point A in Fig. 16) and radome tip (point B in Fig. 16) for different numbers of segmented strips.

6. Discussion

The radome simulations described in this chapter show clearly that the critical electric field magnitude, which is necessary to originate leaders from the aircraft tip, decreases with the aircraft length. The magnitude of the critical electric field decreases from 100 kV/m to 40 kV/m as the aircraft length increases from 20m to 100m. These values are in good agreement with the in-flight measurements of the ambient fields inside storm-cloud (Lalande et al., 1999).

Furthermore, the simulations demonstrated that the electric field inside the radome is not reduced significantly by the radome wall itself, which indicates that the radome does not produce screening effects. This shows that leader can start from the internal electrode (radar

antenna) causing flashover across the radome. Therefore, strips to produce the screening effect must be used to avoid the initiation of streamers from the antenna. The lightning strike to the radome does not damage the radome surface if discharges do not occur from the metal parts inside the radome. This points out that the main purpose of the protection system should be the screening (shielding) of the electric field inside the radome. Poor shielding permits the inception of a discharge from the internal electrode, so the solid strips are usually used to produce the shielding effect. However, effective shielding has undesirable interference effects on antenna radiation. Therefore, the optimal length and number of the strips should be determined.

Significant shielding effect is created by water and ice layers on the radome surface. Under these conditions, the lightning leader can be initiated from the radome tip. Note that the dielectric constant values of ice depend on the frequency of the external field or the rate of voltage rise, and these values affect the electric field magnitude. For example, the values of  $\epsilon_{ice} = 5$  for  $1000 \text{ kV}/\mu\text{s}$  and  $\epsilon_{ice} = 70$  for  $10 \text{ kV}/\mu\text{s}$  were used in (Hardwick et al., 2003). This work has shown that the ice layer does not screen the high frequency radiation associated with the radar.

In high ambient humidity conditions (>60%), the radome becomes moderately conductive because of humidity absorption at its surface (Ulmann et al., 2001; Delannoy et al., 2001). Although this decreases the internal field due to shielding effect, it also reduces the efficiency of the strips.

Numerical simulations have shown that the shielding effect is produced only by solid strips, there is no practical shielding by segmented strips in the absence of a discharge. It was demonstrated that the field intensification area is forced out from the metal electrode (antenna) surface to the front of the radome, thereby preventing discharge initiation from the antenna. However, too strong shielding of antenna surface by increasing the number and the length of strips can cause the field intensification at the frontal area of the radome which can be sufficient to initiate the discharge. Hence, the shielding of the antenna surface as much as possible is not the best solution to the problem. It is necessary to optimize the electric field distribution with respect to the streamer and leader discharge initiation conditions.

Both the fast and slow waveforms (MIL STD 1757 Waveforms A and D respectively) are used for testing radomes (Ulmann et al., 1999). Waveform A has  $1000 \text{ kV}/\mu\text{s}$  rate of rise, and Waveform D has  $50\text{-}250 \mu\text{s}$  rise time. It was concluded (Ulmann et al., 1999) that Waveform D represents the in-flight environment more accurately than Waveform A. For aircraft intercepting approaching leaders, rates of rise of the electric field,  $dU/dt$  of  $10^8$  to  $10^{10} \text{ V/m/s}$  were estimated (Lalande et al., 1999) at the aircraft. If  $1 \text{ MV}/\mu\text{s}$  (waveform A) is applied over a  $1 \text{ m}$  gap, this will give  $dU/dt \approx 10^{12} \text{ V/m/s}$ . Hence, the slower voltage Waveform D tests might be more appropriate. In our tests, we have  $dU/dt \approx U/\tau_i/L \approx 2.8 \cdot 10^5 \text{ V}/2 \cdot 10^{-6} \text{ s}/0.7 \text{ m} \approx 2 \cdot 10^{11} \text{ V/m/s}$ . However, the voltage rise time is important when the voltage is applied directly to the strip. If the high-voltage electrode is placed far from the strip, the breakdown process of the strip is determined by the field generated by the ionization front of the discharge, i.e. by the space charge of the streamers. The magnitude of this field is affected by the velocity of the streamer/leader ionization front, but not by the applied voltage waveform.

Besides direct strikes to aircraft radome, the aircraft could be subjected to indirect strikes. Lightning strike entrance and exit points are usually found at sharp structures of the aircraft, around which the electric field enhancement takes place, but also can occur at any part of the aircraft, including the fuselage, stabilisers, antennas, etc. Observations of such strikes were conducted in a laboratory experiments with aircraft models (Chernov et al., 1992; Petrov et al., 1996). It is seen from Fig. 19, that the nose radome can also be exit point of lightning strike depending on the aircraft position with respect to the approaching lightning threat.

It is worth highlighting here that the lightning diverter strips concept could be adapted for use in protection of ground antennas for ultra-high-frequency communications, which are difficult to protect from direct lightning strikes because interference to the radiation field arises when standard air-terminal shielding is installed (Brael et al., 2004).



Fig. 19. Laboratory testing of lightning strikes to an aircraft model.

## 7. Conclusion

Theoretical analysis and numerical simulations together with experimental laboratory tests of lightning discharge interaction with aircraft radome demonstrated the applicability of existing lightning attachment models to create optimal protection systems against lightning strikes.

The following points can be concluded from the analysis:

- i. Electric field intensification by aircraft flying at high altitudes exceeds the threshold to initiate the lightning leader (50-100 kV/m), this explains why about 90% of lightning strikes to aircraft are initiated by the aircraft.
- ii. The shielding effect of dielectric radome material itself is less than 10%, so the lightning leader can be initiated from the radar antenna.
- iii. The penetration of the electric field, created by the lightning channel or storm-cloud, into the radome is significantly decreased by ice and/or water layers on the radome surface; however, this may cause also the occurrence of punctures.
- iv. Strong diversion effect for the strips comprising isolated metal disks or rings is observed for positive as well as for negative polarity discharges; this type of diverter strip can be used together with the solid strips in order to decrease the interference effect on antenna radiation.
- v. Numerical simulations have shown strong radar shielding effects produced by solid strips and no practical shielding by segmented strips in the absence of a discharge.

## 8. Acknowledgment

N.I.P. and G.N.P. thank colleagues of the High Voltage Group of the Cardiff School of Engineering for hospitality while they worked as guests in their laboratory.

## 9. References

- Amason, M.; et al. (1975). Aircraft application of segmented-strip lightning protection systems, *Proceedings of Conf. on Lightning and Static Electricity*, pp.1-14, London, UK, 1975
- Bruel, C.; Barilleau, D. & Rousseau, A. (2004). Application of aircraft lightning protection to radar stations, *Proceedings of 27<sup>th</sup> Int. Conf. on Lightning Protection*, pp. 975-977, Avignon, France, September 13-16, 2004
- Chernov, E.; Lupeiko, A. & Petrov, N. (1992). Repulsion effect in orientation of Lightning discharge. *J.de Phys. III*, Vol. 2, (July 1992), pp. 1359-1365
- Clifford, D. & Casemir, H. (1982). Triggered lightning. *IEEE Trans. Electromagnetic Compatibility*, Vol. 21, (January 1982), pp. 112-122, ISSN 0018-9375
- Cooray, V.; Rakov, V. & Theethayi, N. (2004). The relationship between the leader charge and the return stroke current – Berger's data revisited, *Proceedings of 27<sup>th</sup> Int. Conf. on Lightning Protection*, pp. 145-150, Avignon, France, September 13-16, 2004
- Delannoy, A.; Bondiou-Clergerie, A.; Lalande, P.; et.al. (2001). New investigations of the mechanisms of lightning strike to radomes Part II: Modeling of the protection efficiency, *Proceedings of Int. Conf. on Lightning and Static Electricity*, paper No 2001-01-2884, Seattle, USA, September 11-13, 2001
- Handbook of Chemistry and Physics. (2001). CRC Press, ISBN 0849304822
- Hardwick, J.; Plumer, A. & Ulmann, A. (1999). Review of the joint radome programme, *Proceedings of ICOLSE'99*, pp.59-65, ISBN 0768003938, Toulouse, France, June 22-24, 1999



- Hardwick, C.; Hawkins, K. & Sanders, M. (2003). Effect of water and icing on segmented diverter strip performance, *Proceedings of ICOLSE'03*, pp. 80.1-80.8, ISBN 1857681525, 9781857681529, Blackpool, UK, September 16-18, 2003
- Larsson, A. (2002). The interaction between a lightning flash and an aircraft in flight. *C.R. Physique*, Vol 3, (December 2002), pp. 1423-1444
- Lalande, P.; Bondiou-Clergerie, A. & Laroche, P. (1999). Analysis of available in-flight measurements of lightning strikes to aircraft, *Proceedings of ICOLSE'99*, pp.401-408, Toulouse, France, June 22-24, 1999
- Mazur, V. (1989). Triggered lightning strikes to aircraft and natural intracloud discharges. *J. Geophys. Res.*, Vol. 94, (March 1989), pp. 3311-3325, ISSN 0148-0227
- Mazur, V. (1989). A physical model of lightning initiation on aircraft in thunderstorms. *J. Geophys. Res.*, Vol. 94, (March 1989), pp. 3326-3340, ISSN 0148-0227
- Mazur, V.; Fisher, B. & Brown, P. (1990). Multistroke cloud-to-ground strike to the NASA F-106B airplane, *J. Geophysical Research*, Vol. 95, no. D5, (May 1990), pp. 5471-5484, ISSN 0148-0227
- Mazur, V. & Moreau, J. (1992). Aircraft-triggered lightning: processes following strike initiation that affect aircraft, *J. Aircr.*, Vol. 29, (August 1992), pp. 575-580, ISSN 0021-8669
- Marshall, T. & Rust, W. (1991). Electric field soundings through thunderstorms. *J. Geophys. Res.*, Vol. 96(22), (December 1991), pp. 297-306, ISSN 0148-0227
- Petrov, N. & Waters, R. (1994). Conductor height and altitude: effect on striking distance, *Proc. Int. Conf. Lightning and Mountains*, pp. 52-57, SEE, Chamonix-Mont-Blanc, June 6-9, 1994.
- Petrov, N. & Waters, R. (1995). Determination of the striking distance of lightning to earthed structures, *Proc. R. Soc. Lond. A*, Vol. 450, No. 1940, (September 1995), pp. 589-601, ISSN 1471-2946
- Petrov, N.; Avansky, V.; Efimova, N. & Petrova, G. (1996). Experimental and theoretical investigations of the orientation of leader discharge to isolated and earthed objects, *Proceedings of 23th Int. Conf. on Lightning Protection*, pp.254-259, Vol.1, Firenze, Italy, September 23-27, 1996
- Petrov, N. & D'Alessandro, F. (2002). Theoretical analysis of the processes involved in lightning attachment to earthed structures, *J. Phys. D: Appl. Phys.*, Vol. 35, No. 14, (July 2002), pp. 1788-1795, ISSN 0022-3727
- Petrov, N. & Waters, R. (1999). Striking distance of Lightning to earthed structures: effect of stroke polarity, *Proc. 11<sup>th</sup> Int. Symp. on High Voltage Engineering*, pp.220-223, Vol. 2, London, UK, August 23-27, 1999
- Plumer, J. & Hoots, L. (1978). Lightning protection with segmented diverters, *Proceedings of IEEE Int. Symp. Electromagnetic Compatibility*, pp.196-203, 1978
- Ulmann, A.; Hardwick, J. & Plumer, A. (1999). Laboratory Reproduction of In-Flight Failures of Radomes, *Proceedings of ICOLSE'99*, pp.493-496, ISBN 0768003938, Toulouse, France, June 22-24, 1999
- Ulmann, A.; Brechet, P.; Bondiou-Clergerie, A.; et.al. (2001). New investigations of the mechanisms of lightning strike to radomes Part I: Experimental study in high

voltage laboratory, *Proceedings of Int. Conf. on Lightning and Static Electricity*, paper No 2001-01-2883, Seattle, USA, September 11-13, 2001

Uman, M. & Rakov, V. (2003). The interaction of lightning with airborne vehicles. *Progress in Aerospace Sciences*, Vol.39, No 1, (January 2003), pp. 61-81, ISSN 0376-0421

IntechOpen

IntechOpen



## **Recent Advances in Aircraft Technology**

Edited by Dr. Ramesh Agarwal

ISBN 978-953-51-0150-5

Hard cover, 544 pages

**Publisher** InTech

**Published online** 24, February, 2012

**Published in print edition** February, 2012

The book describes the state of the art and latest advancements in technologies for various areas of aircraft systems. In particular it covers wide variety of topics in aircraft structures and advanced materials, control systems, electrical systems, inspection and maintenance, avionics and radar and some miscellaneous topics such as green aviation. The authors are leading experts in their fields. Both the researchers and the students should find the material useful in their work.

### **How to reference**

In order to correctly reference this scholarly work, feel free to copy and paste the following:

N.I. Petrov, A. Haddad, G.N. Petrova, H. Griffiths and R.T. Waters (2012). Study of Effects of Lightning Strikes to an Aircraft, Recent Advances in Aircraft Technology, Dr. Ramesh Agarwal (Ed.), ISBN: 978-953-51-0150-5, InTech, Available from: <http://www.intechopen.com/books/recent-advances-in-aircraft-technology/study-of-effects-of-lightning-strikes-to-an-aircraft>

**INTECH**  
open science | open minds

### **InTech Europe**

University Campus STeP Ri  
Slavka Krautzeka 83/A  
51000 Rijeka, Croatia  
Phone: +385 (51) 770 447  
Fax: +385 (51) 686 166  
[www.intechopen.com](http://www.intechopen.com)

### **InTech China**

Unit 405, Office Block, Hotel Equatorial Shanghai  
No.65, Yan An Road (West), Shanghai, 200040, China  
中国上海市延安西路65号上海国际贵都大饭店办公楼405单元  
Phone: +86-21-62489820  
Fax: +86-21-62489821



© 2012 The Author(s). Licensee IntechOpen. This is an open access article distributed under the terms of the [Creative Commons Attribution 3.0 License](https://creativecommons.org/licenses/by/3.0/), which permits unrestricted use, distribution, and reproduction in any medium, provided the original work is properly cited.

IntechOpen

IntechOpen